Numerical structural identification using 3D laser scanning – a simulation-based case study

Eugenio Serantoni[1], Andreas Wieser[2]

[1,2] Institute of Geodesy and Photogrammetry, ETH Zürich, Stefano-Franscini-Platz 5, 8093, Zurich, Switzerland
{eugenio.serantoni, andreas.wieser}@geod.baug.ethz.ch

Key words: *structural health monitoring (SHM); terrestrial laser scanning (TLS); structural identification; finite element method (FEM); integrated monitoring*

ABSTRACT

The integration of areal monitoring techniques such as terrestrial laser scanning (TLS) and the numerical simulation of complex structures is a challenge in the context of structural health monitoring (SHM). Key aspects to facilitate this integration are the thorough handling and modelling of the uncertainties of both measurement and numeric model, and the quantification of the attainable accuracy of the investigated structural parameters depending on the setup configuration.

We give a detailed explanation of an algorithm that integrates the contactless areal monitoring of the surface of a structure and the numerical determination of its material parameters with a finite element (FE) model. The FE mesh is generated automatically from a point cloud acquired using TLS, while the best linear unbiased estimates of unknown material parameters are calculated by matching the displacements predicted with the FE model to the ones derived from laser scans taken at different epochs.

In this contribution, we refine a previously introduced algorithm by (i) explicitly linking the scanned points to the FE mesh, and (ii) taking into account a spatial distribution of uncertainties of the point clouds. Furthermore, we use a closed-loop simulation to study the performance of the algorithm for the case of a simply-supported horizontal beam loaded at midspan and the sensitivity of the results with respect to the scanner location.

I. Introduction

In the realm of structural engineering, terrestrial laser scanning (TLS) is now a technique employed for a variety of tasks such as condition assessment (Mukupa et al., 2017), dimensional control (Kim et al., 2016), automatic generation of models in connection with building information modelling (BIM) (Jung et al., 2015, Brumana et al., 2018), damage inspection (Sánchez-Rodríguez et al., 2018), deformation monitoring (Sarti et al., 2009, Holst et al. 2019), and forward modelling (Bitelli et al., 2018). However, the problem of numerical identification by integrating TLS and finite elements (FE) analysis has not been deeply researched yet, despite its potential in the context of structural health monitoring (SHM). Contributions in this regard have been provided by Wu et al. (2016), Lee et al. (2013), Yang et al. (2018), and by Riveiro et al. (2018). The latter three defined methods to analyse exclusively bent beams.

We have previously published an algorithm (Serantoni et al., 2018) that combines the contactless areal monitoring of a free-form deformable structure and the numerical identification of its mechanical parameters, in the framework of an integrated deformation analysis (Lienhart, 2007). In this paper we present the equations relating the laser scanning observations to the FE model, and address the following questions: which accuracies can be attained? How does the accuracy depend on scanner location and scan resolution? Which are the smallest displacements that the algorithm can correctly process as input?

Chapter 2 contains a concise description of the algorithm. The assessment of the performance of the algorithm for scans acquired from different standpoints is given in chapter 3, as well as a study on the effects of the numerical errors for very small magnitudes of the observation noise. As exemplary application case, we use a bent beam although the applicability of the method is not restricted to this simple case.

II. Method

A. *Outline*

In the framework of an integrated deformation analysis, we have developed a parametric static "white box" model (Welsch & Heunecke, 2001), by merging FE analysis and TLS deformation monitoring. In fact, the FE analysis is a practical and flexible framework to include and integrate measurements from different sensors (Jäger, 2014; Lienhart, 2007). More specifically, in this contribution we focus on a specific identification problem, the determination of material parameters of an elastic object when the applied loads and the resulting deformation are known or have been measured. The flowchart of our algorithm is sketched in figure 1.

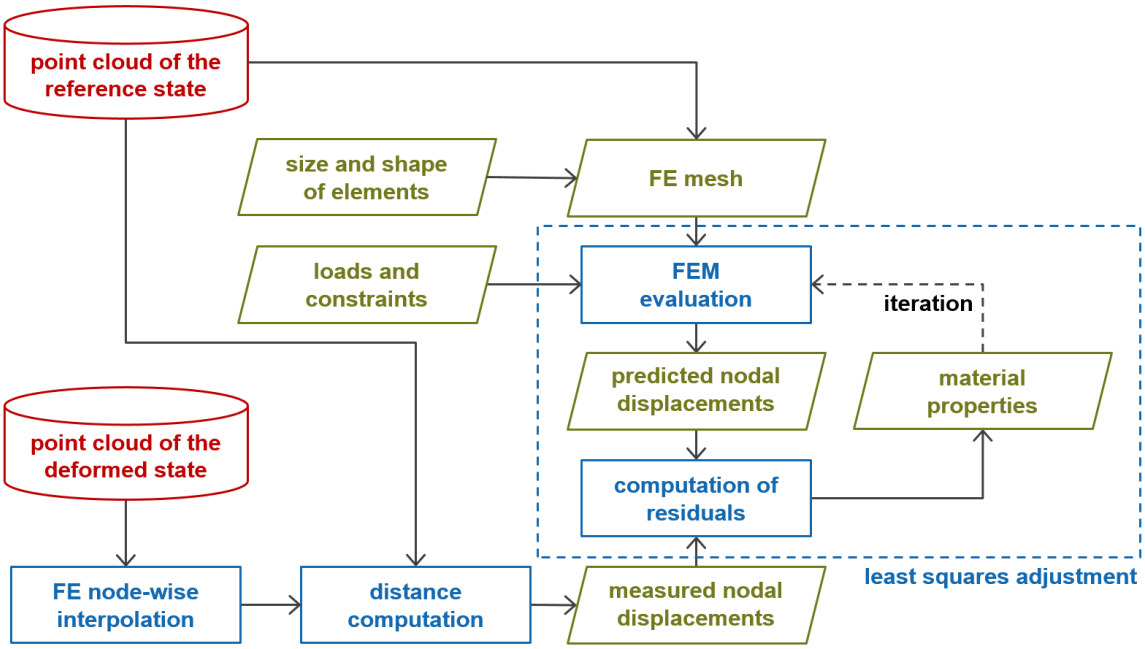

Figure 1. The flowchart of the proposed method.

B. *FE modelling*

When dealing with recently built structures, the FE mesh can often be created from a computer-aided design (CAD) model that is available from the design phase. Extensive work on this topic is available in the literature (e.g. Foucault et al., 2008; Thakur et al., 2009; Gujarathi & Ma, 2010), and the major FE analysis software packages (e.g. Abaqus, Ansys, LS-Dyna, Nastran) already include import tools for CAD geometries. This also holds if the real geometry differs significantly from the CAD model and it is necessary to update it. Conversely, if no prior geometric model is available e.g. for historical structures, the reference point cloud acquired before the deformation can be used to automatically generate a FE mesh of the investigated structure. In this paper, we followed this second approach, by converting the reference point cloud into a FE mesh of 3D elements without employing any CAD software package. We chose to use C3D8 linear bricks because they permit a very straightforward meshing when modelling composite structures made of layers of different materials (Serantoni et al., 2018). The size of the finite elements, and thus their number, has to be determined for each individual application case, finding a trade-off between the desired level of detail and the available computational power. Engineering judgement is particularly important in this stage. For example, when modelling bending members, the size of the finite elements must be small enough to approximate the stress distribution across the cross section. In this contribution we assume the boundary conditions (i.e. loads and constraints) to be known, while the a-priori knowledge of the initial parameters to be estimated can be very rough.

C. *Point cloud acquisition*

The analysis is based on point clouds from two epochs. Herein we assume that a change of loads and thus a potential deformation have occurred between these epochs. We therefore denote the state of the object at the first epoch as "reference state" and at the second epoch as "deformed state" (see figure 1). We also assume that the point clouds are acquired using TLS and we choose a stochastic model accordingly. Actually, the modelling of the variance-covariance matrix (VCM) of TLS point clouds is an open research topic (see e.g. Kauker & Schwieger, 2017) because of the manifold types of errors involved. However, for the sake of simplicity and because we primarily focus on the identification method rather than on the concrete values of the parameters and uncertainties, we model only the instrumental, non-correlating errors, i.e. the angular and range uncertainties of the scanning unit. Moreover, the range accuracy has been assumed to degrade proportionally to the cosine of the incidence angle, as proposed by Soudarissanane (2016). Thus, we use the following model for calculating the standard deviation of the range for each scanned point

$$\sigma_d = \sigma_\rho / \cos\alpha \ , \qquad (1)$$

where σ_d is the standard deviation of the measured distance, σ_ρ is the smallest standard deviation, which is obtained if the laser beam hits the surface orthogonally, and α is the incidence angle of the laser beam.

Additionally, the points are assumed to be uncorrelated and the point clouds are assumed to contain no residual deviations from registration errors (e.g. resulting from mixed pixels). If in a real application

such deviations or errors cannot be ruled out, the point cloud should be carefully checked and filtered in a pre-processing step.

D. *Displacements and their variances*

The deformation of the scanned structure as measured using the laser scanner needs to be related to the displacement of the FE-nodes predicted by the FE analysis. While the point cloud resulting from a scan represents the surface, it is usually not possible to directly relate the individual points of the point cloud to individual physical points on the surface. Thus we propose herein to use the point clouds to calculate the out-of-surface deformation components, i.e. the apparent surface changes perpendicular to the surface at the reference epoch. The approach is thus most sensitive to deformations which actually occur in that direction, e.g. vertical deformation of a horizontal beam loaded on top and scanned from below. While Lienhart (2007) chose to match the predicted and the measured changes in the space of the measurements, we followed the choice of Jäger (2014), who opted for the opposite, namely matching them in the space of nodal displacements. This avoids a computationally costly ray-tracing within each iteration of the least-squares adjustment (LSA) explained in section II.E.

If the point cloud is very dense as compared to the size of the finite elements, it might be sufficient to calculate for each node of the FE mesh just the average of the measured perpendicular displacements of the points in its neighbourhood, together with its associated empirical standard deviation. If instead the distribution of the scanned points is very sparse, i.e. if the average distance between points of the point cloud is greater than about 10% of the size of the finite elements, some more advanced interpolation is necessary. So, the displacement of the surface nodes of the FE mesh along the respective surface normal need to be interpolated from the point clouds. In the example later treated herein, we assume that the surface curvature is negligible as far as the definition of these surface normals is concerned, and that the normals over the entire analysed surface area are approximately parallel to the z-axis of the coordinate system. We can therefore simplify the interpolation of the node-wise perpendicular displacements by projecting the scanned points onto the surface of the reference FE model along the z-axis. The lengths of these projections can then be used as the measured values of the signal to be interpolated.

We have herein chosen to employ a linear triangular interpolation relying on a Delaunay triangulation (Amidror, 2002). Each interpolated displacement δ_N in correspondence of the FE node N is a weighted average of the z coordinates of the three points A, B, C of the point cloud, which form the triangle of the Delaunay triangulation where the node N is projected as N'. The weights are the three normalized areal coordinates of the point N' within the triangle ABC, according to the following formula:

$$\delta_N = \frac{A_{N'BC}}{A_{ABC}} z_A + \frac{A_{N'CA}}{A_{ABC}} z_B + \frac{A_{N'AB}}{A_{ABC}} z_C = \delta_N(x_N, y_N, \mathbf{x})$$
$$\mathbf{x} = [x_A, y_A, z_A, x_B, y_B, z_B, x_C, y_C, z_C]^T, \quad (2)$$

where e.g. A_{ABC} denotes the area of the triangle ABC (see figure 2).

In case of very sparse data and long slim triangles located at the boundaries of the convex hull of the supporting points, this interpolant tends to underestimate the displacement field of bulging surfaces, and vice-versa (Franke, 1982). For accuracy reasons and to circumvent this effect, we avoid extrapolation by excluding from the analysis the FE nodes lying outside the convex hull of the projection of the point cloud onto the FE surface.

Along with the scalar displacements, their variances need to be calculated because they are successively employed in the stochastic model of the parameter estimation. For this purpose, the VCM of the interpolated points have to be calculated along with their coordinates. The most rigorous approach to address such a task is the classic variance propagation starting with the full VCM of the given observations (here the coordinates of the points within the point cloud, after registration to the FE model), including all the correlations among them. However, this solution may be too computationally expensive if the interpolation function is not local and the numerical derivatives required for the variance propagation cannot be derived analytically. In this case numerical differentiation with respect to each of the three coordinates of thousands of points may be necessary when processing the point cloud data. Among the alternatives, also the widespread method of Kriging suffers from the disadvantage of being a "global" method, i.e. the interpolant depends on all the data points (Franke, 1982).

In the interpolation chosen herein (see equation 1) the variance propagation can be performed analytically by derivation of δ_N with respect to all the parameters of the vector $\mathbf{x}$, which contains only the coordinates of the

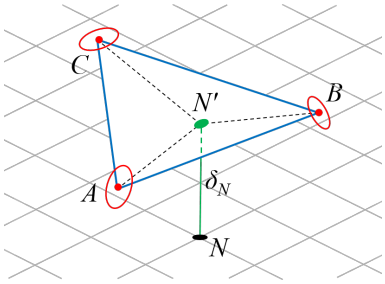

Figure 2. A schematic representation of the linear triangular interpolation. In black, the FE mesh and its nodes; in red, the measured point cloud and the points' error ellipsoids; in blue, the interpolating triangulation; in green, an interpolated point and the calculated distance δ_N.

vertices of a single triangle of the Delaunay triangulation:

$$\sigma^2_{\delta_N} = \left(\frac{\partial \delta_N}{\partial \mathbf{x}}\right)^T \cdot \mathbf{\Sigma}_{ABC} \cdot \left(\frac{\partial \delta_N}{\partial \mathbf{x}}\right), \quad (3)$$

where $\mathbf{\Sigma}_{ABC}$ is a 9x9 VCM including the three VCM of the vertices of the triangle ABC:

$$\mathbf{\Sigma}_{ABC} = \begin{bmatrix} \mathbf{\Sigma}_A & \mathbf{0} & \mathbf{0} \\ \mathbf{0} & \mathbf{\Sigma}_B & \mathbf{0} \\ \mathbf{0} & \mathbf{0} & \mathbf{\Sigma}_C \end{bmatrix} \quad (4)$$

Hereby, we are neglecting the correlation which may occur between interpolated displacements if the respective triangles share one, two or three points, and we neglect the correlations between the coordinates of the triangle's points. Both are simplifications which may be dropped later in case (i) valid and numerically tractable correlation models of the coordinates in a point cloud become available, and (ii) it turns out that taking into account the correlations is necessary for practically useful results.

Other computationally less demanding alternatives are methods based on averaging several positive-semidefinite tensors. Such methods have been developed especially in the field of diffusion tensor imaging for medical applications (e.g. Hotz et al., 2010; Pusz & Woronowicz, 1975), and a review on them is given by Yang et al. (2012). Among them, we propose the log-Euclidean interpolation as presented by Arsigny et al. (2007) because of its particular simplicity and the absence of the Euclidean swelling effect. The latter can be intuitively described as follows: when averaging two symmetric positive-definite matrices, the determinant of the result turns out to be larger than the ones of the original two matrices. More precisely, the log-Euclidean interpolation consists of a weighted average $\bar{\mathbf{\Sigma}}$ of VCMs, according to the following formula,

$$\bar{\mathbf{\Sigma}} = \exp\left(\sum_{i=1}^{N} w_i \ln(\mathbf{\Sigma_i})\right), \quad (5)$$

where the weights w_i are suitably chosen weights, e.g. the normalized areal coordinates shown in formula (1). The natural logarithm of the VCM $\mathbf{\Sigma}$ is obtained by extracting the natural logarithm of each eigenvalue $\mathbf{d_{ij}}$ and successively recomposing the positive-semidefinite matrix as follows:

$$\mathbf{\Sigma} = \mathbf{B}^T \cdot \mathbf{D} \cdot \mathbf{B} \quad (6)$$

$$\tilde{\mathbf{d}}_{\mathbf{ij}} = \begin{cases} \ln(\mathbf{d}_{\mathbf{ij}}) & \text{if } i = j \\ 0 & \text{if } i \neq j \end{cases} \quad (7)$$

$$\ln(\mathbf{\Sigma}) = \mathbf{B}^T \cdot \tilde{\mathbf{D}} \cdot \mathbf{B} \quad (8)$$

Here $\mathbf{B}$ is the square matrix of the eigenvectors, while $\mathbf{D}$ and $\tilde{\mathbf{D}}$ are diagonal matrices of eigenvalues.

The variances $\sigma^2_{\delta_N}$ of the interpolated perpendicular distances are then calculated according to

$$\sigma^2_{\delta_N} = \mathbf{n}^T \cdot \bar{\mathbf{\Sigma}} \cdot \mathbf{n}, \quad (9)$$

where $\mathbf{n}$ is the unit vector in the direction of displacement. The result we obtain with this approach is an approximation of the set of VCMs that we would expect if the scanned points would coincide with the projections of the FE nodes onto the interpolated surface.

E. *Parameter estimation*

The core of the algorithm is the iterative match of the measured and the predicted nodal displacements. The matching is conducted with an ordinary Gauss-Markov LSA that finds the best linear unbiased estimator of the sought material properties, according to the following formulas.

$$\hat{\boldsymbol{\xi}} = (\mathbf{A^T P A})^{-1} \mathbf{A^T P y} \quad (10)$$

$$\mathbf{\Sigma}_{\hat{\xi}\hat{\xi}} = \sigma_0^2 (\mathbf{A^T P A})^{-1} \quad (11)$$

$$\mathbf{P} = \sigma_0^{-2} \mathbf{\Sigma}_{\mathbf{yy}}^{-1} \quad (12)$$

Here, $\mathbf{A}$ is the design matrix and it contains the numerical derivatives of the nodal displacements with respect to the sought material parameters $\hat{\boldsymbol{\xi}}$, $\mathbf{P}$ is the weight matrix, σ_0^2 is the a-priori variance factor, $\mathbf{\Sigma}_{\mathbf{yy}}$ and $\mathbf{\Sigma}_{\hat{\xi}\hat{\xi}}$ are the VCMs of the measured nodal displacements and of the estimated parameters, respectively. $\mathbf{\Sigma}_{\mathbf{yy}}$ is herein assumed to be diagonal and contains the variances $\sigma^2_{\delta_N}$ of the displacements, according to the methods shown in the section II.D., while the vector $\mathbf{y}$ represents the observed displacements δ_N.

At the present stage, this adjustment is not a fully integrated monitoring method, because the measurements are retrieved from a single measurement unit, and the boundary conditions are assumed perfectly known. However, this represent a preparatory study to fully integrate TLS measurements in the framework of integrated monitoring.

III. NUMERICAL STUDY

In order to demonstrate the method presented herein and to show how it can be used for a configuration assessment similar to the one carried out as part of the preanalysis of geodetic network, we created a closed-loop numerical simulation tool. It comprises the generation of synthetic TLS point clouds from an FE model of a structure, assumed loads and an assumed location of the scanner. These point clouds are then processed together with an FE model only approximately equal to the one used for point cloud generation. The resulting material parameters, e.g. Young's moduli $\hat{E}$, and their standard deviations $\sigma_{\hat{E}}$ are then compared to the ground truth values. We chose to conduct simulations instead of real measurements in order to better control the boundary conditions and the observation noise levels, to have nearly arbitrary flexibility regarding shape and material

properties of the object, and to know the ground truth for assessing the accuracy.

A. *Experimental setup for a single sensor location*

The application example presented herein has been designed with the following requirements in mind: (i) maximum displacements larger than the accuracy typically achieved with a terrestrial laser scanner over distances of a few meters (ca. 2-5 mm), (ii) compliance with the assumption of linear elastic material avoiding local plasticity effects (e.g. cracks, plastic hinges) by keeping the stress below the yield point in the whole structure, (iii) easy reproducibility in a lab, in case of future real experiments. Therefore, we modelled a 2 m long, simply supported flat bar (E_0 = 210 GPa, Poisson ratio = 0, density = 7850 kg/m^3), with a cross section 150 mm wide and 25 mm high. The self-weight of the bar is taken into account. The bar is subject to a three-point flexural test without torsion, and the vertical load at mid-span (4 kN, marked as **F** in figure 3) has been distributed over the whole cross section, in order to minimise local deformation effects and to approximate the ideal case of a simply-supported slender beam. In this way, we could better validate the results.

The simulated scans have a resolution in both azimuth and elevation angle of 0.6 gon and cover the extrados of the beam, i.e. the bottom surface, where the longitudinal fibres experience traction. We do not create and process simulated scan data of the sides of the beam because there would be almost exclusively in-plane displacement of surface points for these sides, and the laser scan is not sensitive with respect to them. As for the standard deviations of the measurements, we assumed the arbitrary but realistic values of 0.5 mgon for all angles, and of 2 mm for σ_ρ, according to equation (1). For this analysis the coordinate system has been defined such that the centre of the beam extrados lies in the point (0, 0, 2.5), the y-axis is parallel to the long edge of the beam, and the xy-plane is parallel to the bottom and top surface of the beam (see figure 3).

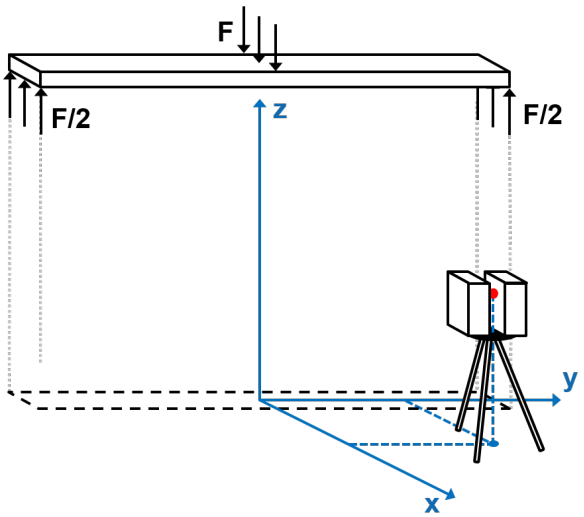

Figure 3. Sketch of the experimental setup, including the system of coordinates (in blue) and the sensor location (in red). The sketch is not drawn to scale.

As first experiment, we estimated E using 100 synthetic point clouds acquired for the scanner location (0, 0, 0) with random azimuthal orientation. We obtained an average $\hat{E}$ of 210.71 GPa, which deviates only 0.3% from the ground truth; the empirical standard deviation of the 100 samples is 3.4 GPa. The estimated standard deviation $\sigma_{\hat{E}}$, obtained directly from the LSA, is smaller by a factor of 4-7 for most realizations, indicating that the simplified variance propagation discussed above may have to be revisited.

B. *Multiple sensor locations*

We have repeated the estimation of E for several sensor locations in the vicinity of the beam. As the beam and the applied forces have two perpendicular axes of symmetry parallel to the xy plane, only scanner locations belonging to a single quadrant have actually been simulated, concretely 64 locations forming a non-regular 8x8 grid (see dots in figure 4), which lies on a horizontal plane 2.5 m below the extrados of the beam.

The outcomes of the simulations by using the variance propagation illustrated with formula (3) show that standpoints farther than 8 m deliver a strong bias because of the small number of scanned points still covering the extrados (less than 25). Moreover, in these areas, our approach generally overestimates $\hat{E}$ because of an underestimation of the nodal displacements due to the sparse data and the linear interpolation method (see section II.D.).

In order to compare the two presented methods for the interpolation of VCMs, we show the respective results on a smaller area of 4x4 m^2 (figure 5). We observe that the results obtained using the log-

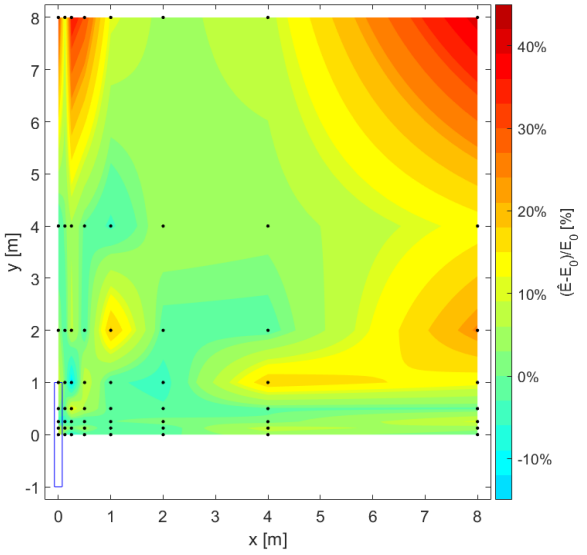

Figure 4. Deviation of the estimated value $\hat{E}$ as percent ratio of the ground truth E_0. The scanned beam is outlined in blue and the black dots represent the simulated standpoints, while the colours are interpolated between them.

Euclidean method are smoother than the ones obtained with the simplified variance propagation, with a maximum bias of 7.6% (figure 5b) and 20.0% (figure 5a), respectively. A possible reason could be the effect of observation noise in the computation of the partial derivatives for the variance propagation-based approach. However, this hypothesis should be supported by future detailed investigations.

Moreover, as figures 5c and 5d show, the predicted standard deviation $\sigma_{\hat{E}}$ is less than 1% of E_0 for all scanner locations taken into account. This is much smaller than the biases shown in figures 5a and 5b, indicating that the biases are not negligible. Bias and estimated uncertainty are apparently related, as the contour lines in figures 5a and 5c, and 5b and 5d respectively show. Not surprisingly, the standpoints aligned with the longitudinal axis of the beam are the ones delivering the most unstable results. For these points a small change of configuration can cause a large change in the amount of scanned points on the bottom surface of the beam. In fact, at a large distance, apart from the problems caused by an unfavorable angle of incidence, only one row of scanned points might be on that surface.

The comparison with similar analyses conducted by other authors is difficult because of the different experimental setups. However, we encounter biases on $\hat{E}$ larger than 13.3%, as obtained e.g. in Riveiro et al. (2018), who also analysed the identification of E for a loaded horizontal beam. Future work will have to identify whether our approach really yields higher accuracy (and if so, how much of it is due to the assumption of known boundary conditions) or whether the predicted accuracy of our approach is too optimistic.

C. *Influence of numerical errors*

A separate brief analysis for numerical stability showed that the algorithm and the LSA work properly for standard deviations of the coordinates within the point clouds of 0.01 mm. For smaller noise levels the standard deviations of the solution are dominated by quantization errors of the input data. If a scanner of such high precision were available, the Young modulus could be determined with a bias below 0.2% and a

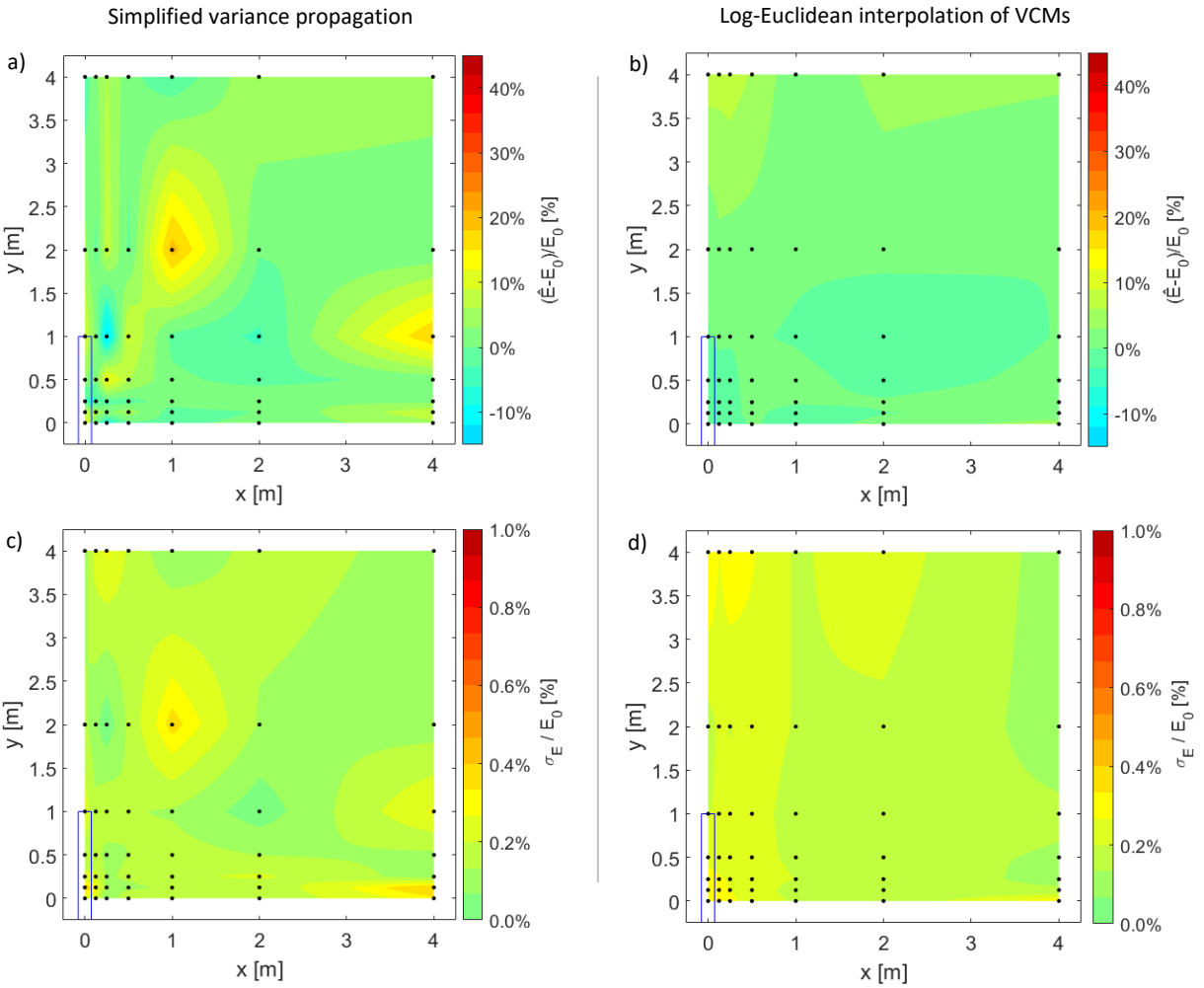

Figure 5. Results of the simulation for multiple standpoints. a, c) deviation of the estimated value $\hat{E}$ from E_0; b, d) estimated standard deviation σ_E of the Young modulus. Values expressed as percent ratios to the ground truth E_0. The scanned beam is outlined in blue and the black dots represent the simulated standpoints, while the colours are interpolated between them.

standard deviation below 0.1 GPa using the case described in section III.A; this is a lower bound of the achievable precision with the current algorithm and current formats for data transfer between the various software components.

IV. Conclusion and outlook

With this contribution we showed how we refined and tested our algorithm for numerical identification of material parameters of a structure using terrestrial laser scanning and finite element modelling. The core elements are the calculation of surface-deformations orthogonal to the surface from the laser scans, the interpolation of these deformations to the surface nodes of the finite element model (FEM), and the iterated adaptation of the parameters of the FEM until the discrepancies between the predicted node displacements and the measured ones match best in consideration of the VCM of the scanned points, and analysed the situation of Young's modulus estimated from a horizontal steal bar loaded at its centre. Using a closed-loop simulation and assuming the loads to be known at two epochs at which scans are made, we obtained a bias below 0.3% and a standard deviation of about 1.7% for Young's modulus, based on a set of scans from beneath the centre of the beam.

Moreover, we analysed the impact of scanning location with respect to the beam and found that the precision and bias quickly degrade once the scanner moves away from beneath the bar. This degradation is due to increased scanning noise and decreasing number of points on the surface of the bar with increasing distance and angle of incidence. However, the analysis did not take into account systematic deviations of the scanning due to angle of incidence, surface roughness or similar effects; it is therefore to be expected that the results degrade even more with real scanning data than in our simulation. The presented analytical approach based on closed-loop simulation can be easily modified in order to assess the influence of other variable characteristics of the experimental setup e.g. scanner resolution or scanner accuracy. The scan-based identification can of course be extended to structures beyond beams, and by extending it to a full integrated analysis jointly estimating parameters, loads and deformation, can be a powerful tool for structural health monitoring.

V. Acknowledgements

We thank Geo Boffi and Zan Gojcic for useful input on an earlier version of this contribution.

References

Amidror, I. (2002). Scattered data interpolation methods for electronic imaging systems: a survey. Journal of electronic imaging, 11(2), 157-177.

Arsigny, V., Fillard, P., Pennec, X., & Ayache, N. (2007). Geometric means in a novel vector space structure on symmetric positive-definite matrices. SIAM journal on matrix analysis and applications, 29(1), 328-347.

Bitelli, G., Castellazzi, G., D'Altri, A. M., de Miranda, S., Lambertini, A., & Selvaggi, I. (2018). On the generation of numerical models from point clouds for the analysis of damaged Cultural Heritage. In IOP Conference Series: Materials Science and Engineering, 364(1).

Brumana, R., Della Torre, S., Previtali, M., Barazzetti, L., Cantini, L., Oreni, D., & Banfi, F. (2018). Generative HBIM modelling to embody complexity (LOD, LOG, LOA, LOI): surveying, preservation, site intervention—the Basilica di Collemaggio (L'Aquila). Applied Geomatics, 10(4), 545-567.

Foucault, G., Cuillière, J. C., François, V., Léon, J. C., & Maranzana, R. (2008). Adaptation of CAD model topology for finite element analysis. Computer-Aided Design, 40(2), 176-196.

Franke, R. (1982). Scattered data interpolation: tests of some methods. Mathematics of computation, 38(157), 181-200.

Gujarathi, G. P., & Ma, Y. S. (2010). Generative CAD and CAE integration using common data model. In 2010 IEEE International Conference on Automation Science and Engineering, 586-591.

Holst, C., Nothnagel, A., Haas, R., & Kuhlmann, H. (2019). Investigating the gravitational stability of a radio telescope's reference point using a terrestrial laser scanner: Case study at the Onsala Space Observatory 20-m radio telescope. ISPRS Journal of Photogrammetry and Remote Sensing, 149, 67-76.

Hotz, I., Sreevalsan-Nair, J., Hagen, H., & Hamann, B. (2010). Tensor field reconstruction based on eigenvector and eigenvalue interpolation. In Dagstuhl Follow-Ups, 1, Schloss Dagstuhl-Leibniz-Zentrum fuer Informatik.

Jäger, R. (2014) Methods and Approaches for Integrated deformation Analysis. In: Proceedings of the International Workshop Integration of Point- and Area-wise Geodetic Monitoring for Structures and Natural Objects, Novosibirsk, Russian Federation, 32-52.

Jung, J., Hong, S., Yoon, S., Kim, J., & Heo, J. (2015). Automated 3D wireframe modeling of indoor structures from point clouds using constrained least-squares adjustment for as-built BIM. Journal of Computing in Civil Engineering, 30(4).

Kauker, S., & Schwieger, V. (2017). A synthetic covariance matrix for monitoring by terrestrial laser scanning. Journal of Applied Geodesy, 11(2), 77-87.

Kim, M. K., Wang, Q., Park, J. W., Cheng, J. C., Sohn, H., & Chang, C. C. (2016). Automated dimensional quality assurance of full-scale precast concrete elements using laser scanning and BIM. Automation in Construction, 72, 102-114.

Lee, H. M., & Hyo, S. P. (2013). Stress Estimation of Beam Structures Based on 3D Coordinate Information from Terrestrial Laser Scanning. In Third International Conference on Control, Automation and Systems Engineering (CASE-13).

Lienhart, W. (2007). Analysis of Inhomogeneous Structural Monitoring Data, Dissertation, Graz University of Technology.

Mukupa, W., Hancock, C., Roberts, G., Al-Manasir, K., de Ligt, H., & Chen, Z. (2017). Visual inspection of fire-damaged concrete based on terrestrial laser scanner data. Applied Geomatics, 9(3), 143-158.

Pusz, W., & Woronowicz, S. L. (1975). Functional calculus for sesquilinear forms and the purification map. Reports on Mathematical Physics, 8(2), 159-170.

Riveiro, B., Cubreiro, G., Conde, B., Cabaleiro, M., Lindenbergh, R., Soilán, M., & Caamaño, J. C. (2018). Automated calibration of fem models using LiDAR point clouds. International Archives of the Photogrammetry, Remote Sensing and Spatial Information Sciences, 42(2).

Sánchez-Rodríguez, A., Riveiro, B., Conde, B., & Soilán, M. (2018). Detection of structural faults in piers of masonry arch bridges through automated processing of laser scanning data. Structural Control and Health Monitoring, 25(3).

Sarti, P., Vittuari, L., & Abbondanza, C. (2009). Laser scanner and terrestrial surveying applied to gravitational deformation monitoring of large VLBI telescopes' primary reflector. Journal of Surveying Engineering, 135(4), 136-148.

Serantoni, E., Muster, M., & Wieser, A. (2018). Numerical structural identification of a cross-laminated timber slab using 3D laserscanning. In: 9th European Workshop on Structural Health Monitoring (EWSHM 2018), Manchester, UK.

Soudarissanane, S. S. (2016). The geometry of terrestrial laser scanning; identification of errors, modeling and mitigation of scanning geometry, Dissertation, TU Delft

Thakur, A., Banerjee, A. G., & Gupta, S. K. (2009). A survey of CAD model simplification techniques for physics-based simulation applications. Computer-Aided Design, 41(2), 65-80.

Welsch, W., & Heunecke, O. (2001). Models and terminology for the analysis of geodetic monitoring observations. International Federation of Surveyors.

Wu, C. C., Weisbrich, S., & Neitzel, F. (2016). Inverse finite element adjustment of material parameters from integrated analysis of displacement field measurement. Materials Today: Proceedings, 3(4), 1211-1215.

Yang, F., Zhu, Y. M., Magnin, I. E., Luo, J. H., Croisille, P., & Kingsley, P. B. (2012). Feature-based interpolation of diffusion tensor fields and application to human cardiac DT-MRI. Medical image analysis, 16(2), 459-481.

Yang, H., Xu, X., & Neumann, I. (2018). Optimal finite element model with response surface methodology for concrete structures based on Terrestrial Laser Scanning technology. Composite Structures, 183, 2(6).